NACA RM L53K17

NACA

RESEARCH MEMORANDUM

TRANSONIC DRAG MEASUREMENTS OF EIGHT BODY-NOSE SHAPES

By William E. Stoney, Jr.

Langley Aeronautical Laboratory
Langley Field, Va.

NATIONAL ADVISORY COMMITTEE
FOR AERONAUTICS
WASHINGTON

February 5, 1954
Declassified October 14, 1957

NACA RM L53K17

NATIONAL ADVISORY COMMITTEE FOR AERONAUTICS

RESEARCH MEMORANDUM

TRANSONIC DRAG MEASUREMENTS OF EIGHT BODY-NOSE SHAPES

By William E. Stoney, Jr.

SUMMARY

Zero-lift drag data were obtained on a series of eight fin-stabilized bodies having fineness-ratio-3 noses and differing only in nose shape. The models were launched from the Langley helium gun (at the testing station at Wallops Island, Va.) and data were obtained for Mach numbers from 0.8 to 1.25 with corresponding Reynolds numbers (based on body length) of 8×10^6 to 15×10^6.

The results were compared with theoretical calculations and with wind-tunnel measurements. Lowest transonic drag values were obtained with nose shapes defined by the Von Kármán optimum and by a parabola with its vertex at the nose tip.

INTRODUCTION

At supersonic speeds the pressure drag of the nose of a body may be an appreciable part of the total drag. This is especially true for noses whose fineness ratio is low (less than 5) which may be necessary for various design conditions. Because of the importance of nose shape on the drag of noses, tests were conducted on a series of fineness-ratio-3 nose shapes for Mach numbers from 1.24 to 3.67 at the Ames Aeronautical Laboratory and results were presented in reference 1. The results showed good agreement with second-order theory (ref. 2) above a Mach number of 1.4. Since theoretical calculations, in general, either gave poor results or could not be made at all at lower Mach numbers, the present tests were initiated to determine experimentally the nose pressure drags in the transonic and low supersonic speed range. The nose shapes selected for testing were chosen because they were the results of various "optimum calculations," had shown low drag in the tests at the Ames Laboratory, or were in general use.

The fineness ratio of 3 was chosen so that the resulting drag differences would be large enough to measure and to allow direct comparison

with the data of reference 1. This fineness ratio is definitely not recommended for low-drag supersonic bodies.

Data were obtained for a Mach number range from 0.8 to 1.25 and a Reynolds number range from 8×10^6 to 15×10^6 based on body length.

The data are presented herein with only brief analysis in order to expedite their publication.

SYMBOLS

$r = \dfrac{\text{Radius}}{\text{Maximum radius}}$

$x = \dfrac{\text{Distance from nose}}{\text{Total nose length}}$

l length

d maximum diameter

$C_d = \dfrac{\text{Drag}}{q \times \text{Maximum frontal area}}$

$C_{d_f} = \dfrac{\text{Friction drag}}{q \times \text{Maximum frontal area}}$

$C_f = \dfrac{\text{Friction drag of equivalent flat plate}}{q \times \text{Wetted area}}$

$P = \dfrac{\text{Local pressure - Free-stream static pressure}}{q}$

q dynamic pressure

MODELS AND TESTS

The test configurations are shown in figure 1, and photographs of all the models are presented in figure 2. The basic configuration (fig. 1(a)) behind the nose section was the same for all models. The nose section was followed by a cylindrical section of $l/d = 4$ to which was attached a conical afterbody of $l/d = 5$. The models were made of wood and the fins were aluminum.

The nose shapes tested were all of fineness ratio 3 and may conveniently be divided into three groups (fig. 1(b)).

Power Series

These nose shapes are defined by the equation

$$r = x^n \qquad (0 \leq x \leq 1)$$

The three noses of the power series had values of $n = 1$, $3/4$, and $1/2$. Note that for $n = 1/2$ the equation describes a parabola with the vertex at $x = 0$.

Parabolic Series

These meridians are defined by the equation

$$r = \frac{2x - Kx^2}{2 - K} \qquad (0 \leq x \leq 1)$$

Three noses of the parabolic series having the following values of K were tested. The cone may also be considered a member of this family with $K = 0$

Parabolic

$K = 1$

$\frac{3}{4}$P

$K = 0.75$

$\frac{1}{2}$P

$K = 0.5$

Haack Series

The meridians of the Haack series are defined as follows

$$r = \frac{1}{\sqrt{\pi}} \sqrt{\phi - \frac{1}{2} \sin 2\phi + C \sin^3 \phi}$$

where

$$\phi = \cos^{-1} (1 - 2x) \qquad (0 \leq x \leq 1)$$

Two noses having the following values of C were tested:

Von Kármán

$$C = 0$$

L-V Haack

$$C = 1/3$$

The Von Kármán nose is also called the L-D Haack nose in reference 1. The letters L-D and L-V refer to the boundary conditions for which the drag was minimized. The former signifies given length and diameter and the latter given length and volume.

The models were fired from the Langley helium gun (at the testing station at Wallops Island, Va.) which is described in reference 3 and the data were reduced in the manner described in reference 4. Data were obtained over a range of Mach numbers from 0.8 to 1.25 and for Reynolds numbers (based on body length) between 8×10^6 and 15×10^6.

The accuracy of the data as estimated from experience with previous models is of the order of ±0.008 in total C_D and ±0.005 in M.

RESULTS AND DISCUSSION

Total-Configuration Drag

The drag coefficients for the test configurations are presented as a function of Mach number in figure 3. Also shown are values of the body-plus-fin-friction drag coefficients calculated by the method of

Van Driest (ref. 5) assuming completely turbulent boundary-layer flow. The difference between these friction values and the subsonic ($M \approx 0.8$) total-drag curves is about the same for all models ($C_d \approx 0.025$) except for the conical nose body. This constant difference may be attributed to base pressure drag and to body pressure drag caused by the cutoff base. The drag difference noted indicates base pressure coefficients of the order of $P = -0.13$ and thus close to the value of $P = -0.125$ obtained on the base of a cylindrical afterbody (ref. 6). This is reasonable since the present afterbody is long and its slope is small (1.63°). The higher subsonic drag of the conical model may be due to additional pressure drag caused by the sharp angle (9.48°) at the nose-cylinder juncture. It is reasonable to assume from the above comparisons that all the models had turbulent boundary-layer flow throughout the test Mach number range.

Nose Pressure Drag

In order to present the test results in a form more applicable to general use and to allow comparison with the data of reference 1, it is necessary to separate the nose pressure drags from the drags of the total configurations. The nose pressure drags obtained are directly applicable to the drag of such noses on any body shape at supersonic speeds although their effect on the flow field over the afterbody must be considered in a total-drag estimation. At transonic and subsonic speeds the isolated nose drags derived herein will be correct only for bodies which approximate the test configuration.

In order to obtain these nose pressure drags the following assumptions were made. These pertain to the conditions at supersonic speeds.

(1) The different pressure fields of the various nose shapes do not appreciably affect the pressure drags of the afterbody, fins, or base. This relative independence of the afterbody pressures appears reasonable from the linear calculations of reference 7 since the nose is separated from the afterbody and tail by a fineness-ratio-4 cylinder. The effect on total drag of even large percentage changes in fin pressure drag would be small since their isolated pressure drag is of the order of 7 percent of the total supersonic drag.

(2) The sum of the afterbody, fin, and base drags, which has been assumed the same for all models, may be obtained by subtracting a known nose pressure drag from any of the models. The tare drag coefficient so obtained does not vary appreciably with Mach number in the supersonic range.

The tare drag presented in figure 4 is equal to the sum of the afterbody, fin, and base pressure drags. The value at $M = 1.2$ was

obtained by subtracting from the total drag the sum of the calculated friction drag and the pressure drag for the cone obtained by the theoretical calculations of reference 8. The subsonic level was assumed to be the constant value of 0.025 shown previously. The curve was completed by fairing the $M = 1.2$ value to peak-drag and drag-rise Mach numbers estimated from the data obtained with a configuration having the same fineness-ratio-5 afterbody as the present models but headed by a fineness-ratio-7.13 parabolic nose (ref. 4). The value of the tare drag at $M = 1.2$ obtained in the above manner agreed well with that obtained from this reference body.

The tare drag having been determined, the procedure was reversed and the nose pressure drags were obtained for all the noses tested. The resulting drags are shown in figure 5 attached to and compared with the higher Mach number data of reference 1 and with the theoretical values obtained by the method of reference 2. The lines connecting the data from reference 1 have been faired and in some cases represent a compromise between the two sets of data.

The agreement of the data obtained in the present tests with those of reference 1 is within the combined accuracy of the two test techniques for all models with the exception of the $x^{1/2}$ body. The agreement of the parabolic series with the second-order calculations of reference 2 appears to be quite good also.

The drag coefficients shown are based on the maximum frontal area. To allow easy estimations of the relative effect of the various nose shapes on the friction drag and on the drag per unit volume, the nondimensional factors obtained from the following equations are presented in the subsequent table.

$$\frac{C_{D_f}}{C_f} \frac{1}{4l/d} = \int_0^1 r \, dx \tag{1}$$

$$\frac{\text{Volume}}{\pi d^2 l/4} = \int_0^1 r^2 dx \tag{2}$$

For bodies of normal fineness ratio the expression of equation (1) gives substantially the same numbers as the more usual equation

$$\frac{C_{D_f}}{C_f} = \frac{\text{Wetted area}}{\text{Frontal area}}$$

Equation (1) is, however, the correct one in that it sums only the drag components of the friction force, whereas the other includes those components normal to the axis of symmetry as well.

The nondimensional factors determined by the above equations are:

Nose shapes	$\frac{C_{D_f}}{C_f}\frac{l}{4l/d}$	$\frac{\text{Volume}}{\pi d^2 l/4}$
Cone	0.500	0.333
$x^{3/4}$	.571	.400
$x^{1/2}$	.667	.500
Parabolic	.667	.534
$\frac{3}{4}$P	.600	.445
$\frac{1}{2}$P	.556	.393
L-V Haack	.700	.562
Von Kármán	.653	.500

CONCLUDING REMARKS

The present results together with the results of NACA RM A52H28 indicate that the Von Kármán and the $x^{1/2}$ noses have the lowest drag over most of the Mach number range (M = 0.8 to 2). While the $x^{1/2}$ nose apparently had a low initial drag rise, its drag continues to rise slowly over most of the Mach number range shown. This appears to be a result of its extremely blunt apex. The drag of the Von Kármán nose however peaks at about M = 1.4, after which Mach number it decreases with increasing M. This characteristic of decreasing drag coefficient at high supersonic Mach numbers is also shown by the $x^{3/4}$ nose. In fact this nose $(x^{3/4})$ approximates closely that derived for minimum hypersonic drag for given length and diameter (see NACA RM A52H28) and it is interesting to note that in the limit as $x \longrightarrow 0$ the equation for the Von Kármán nose approaches $r = x^{3/4}$ (where r is the ratio of radius to maximum radius and x is the ratio of the distance from the nose to total nose length). The Von Kármán nose has the further advantage of fairing smoothly into the body behind it which apparently is a factor in obtaining low subsonic drag and high drag-rise Mach numbers. It also seems reasonable to assume that this factor would also tend to

reduce the interference drag of the nose on an afterbody in comparison with noses having finite slopes at the nose-afterbody juncture.

These tests of noses of fineness ratio 3 are not intended to imply that this fineness ratio is considered a good one from the point of view of low supersonic drag. The effect of fineness ratio on the comparative results of these noses is not known; however, it appears reasonable to assume that, for the low fineness ratios where the pressure drag will be fairly high (fineness ratio of approximately 5 or 6), the comparisons measured here at a fineness ratio of 3 will be essentially correct; above fineness ratios of 5 or 6, the pressure drag becomes less important and so probably does nose shape.

Langley Aeronautical Laboratory,
National Advisory Committee for Aeronautics,
Langley Field, Va., November 3, 1953.

REFERENCES

1. Perkins, Edward W., and Jorgensen, Leland H.: Investigation of the Drag of Various Axially Symmetric Nose Shapes of Fineness Ratio 3 for Mach Numbers From 1.24 to 3.67. NACA RM A52H28, 1952.

2. Van Dyke, Milton Denaan: Practical Calculation of Second-Order Supersonic Flow Past Nonlifting Bodies of Revolution. NACA TN 2744, 1952.

3. Hall, James Rudyard: Comparison of Free-Flight Measurements of the Zero-Lift Drag Rise of Six Airplane Configurations and Their Equivalent Bodies of Revolution at Transonic Speeds. NACA RM L53J21a, 1953.

4. Stoney, William E., Jr.: Some Experimental Effects of Afterbody Shape on the Zero-Lift Drag of Bodies for Mach Numbers Between 0.8 to 1.3. NACA RM L53I01, 1953.

5. Van Driest, E. R.: Turbulent Boundary Layer in Compressible Fluids. Jour. Aero. Sci., vol. 18, no. 3, Mar. 1951, pp. 145-160, 216.

6. Katz, Ellis R., and Stoney, William E., Jr.: Base Pressures Measured on Several Parabolic-Arc Bodies of Revolution in Free Flight at Mach Numbers from 0.8 to 1.4 and at Large Reynolds Numbers. NACA RM L51F29, 1951.

7. Fraenkel, L. E.: The Theoretical Wave Drag of Some Bodies of Revolution. Rep. No. Aero. 2420, British R.A.E., May 1951.

8. Staff of the Computing Section, Center of Analysis (Under Direction of Zdeněck Kopal): Tables of Supersonic Flow Around Cones. Tech. Rep. No. 1, M.I.T., 1947.

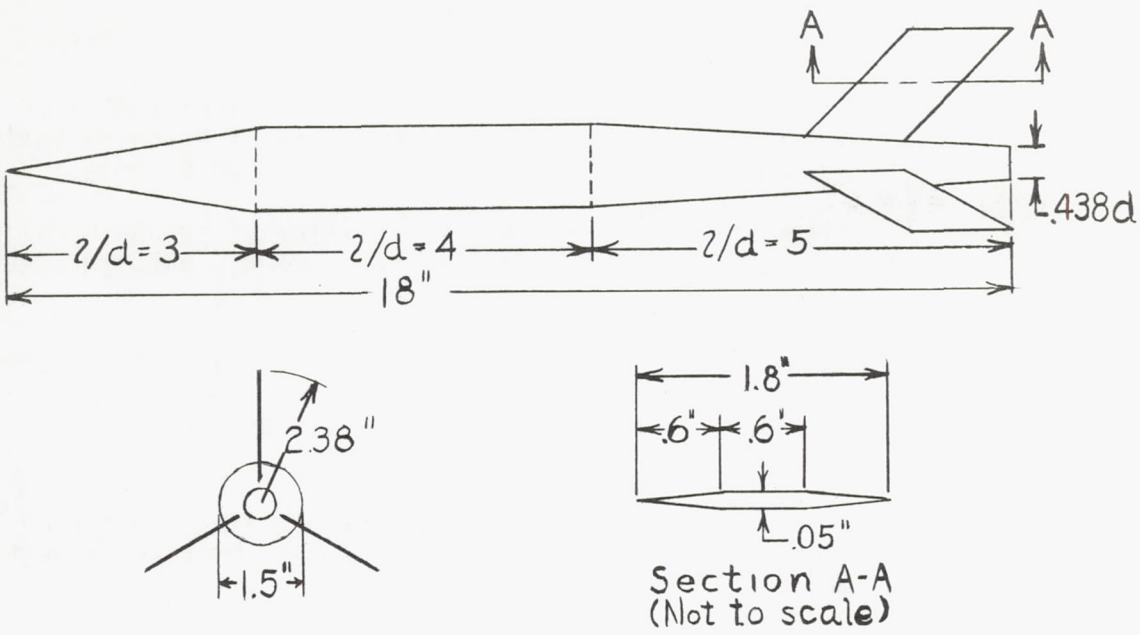

(a) Basic configuration.

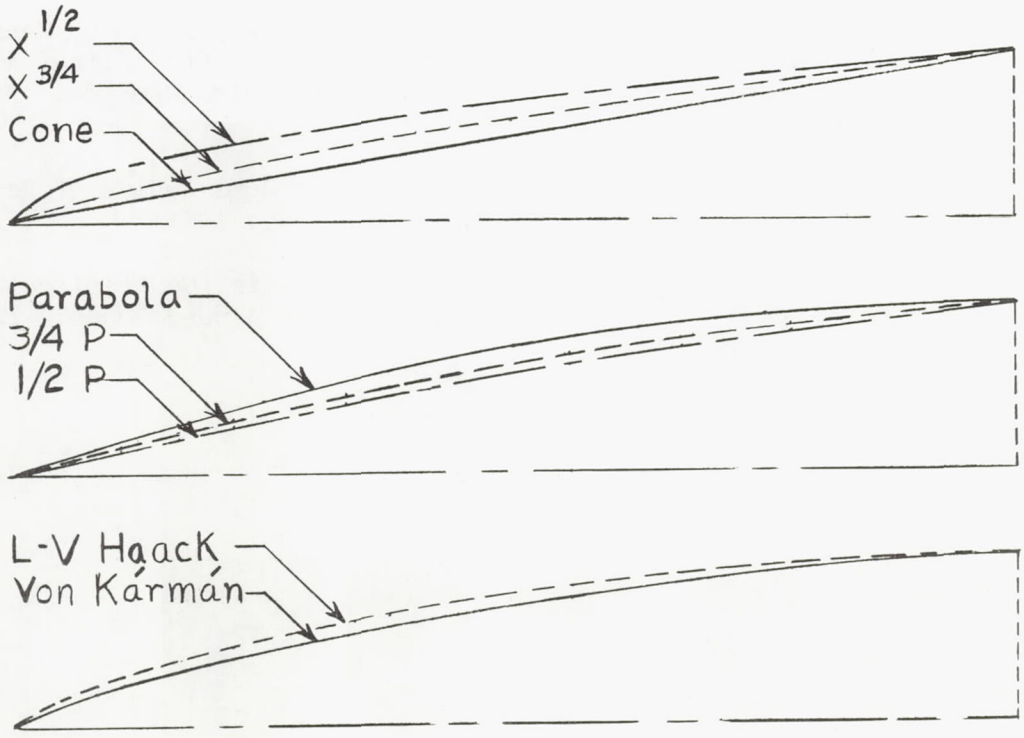

(b) Nose shapes.

Figure 1.- Test configurations.

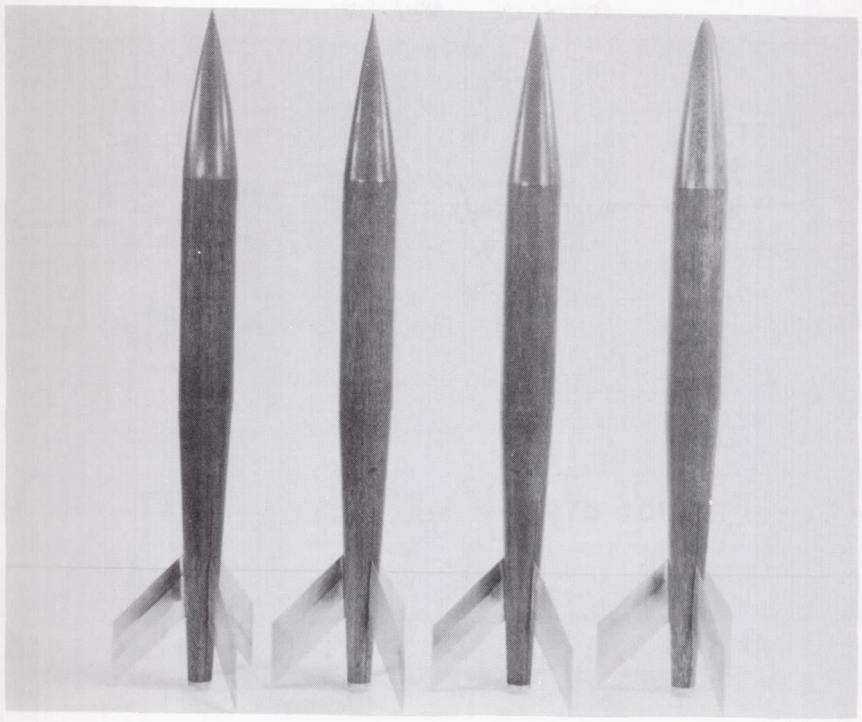

$\frac{3}{4}P$ $\frac{1}{2}P$ $x^{3/4}$ $x^{1/2}$ L-79629

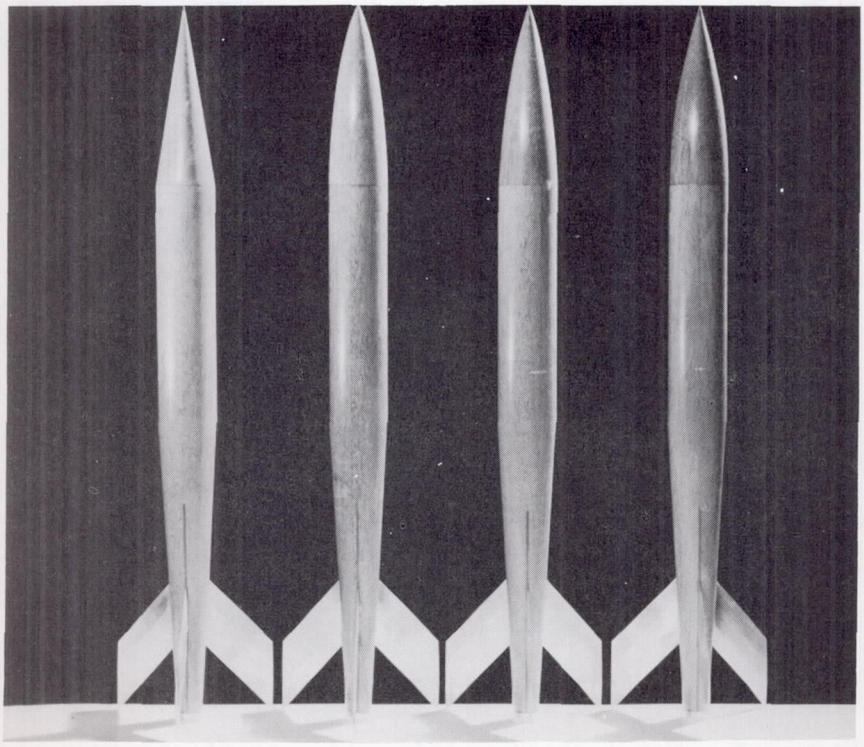

Cone L-V Haack Von Kármán Parabola L-79889

Figure 2.- Photographs of models.

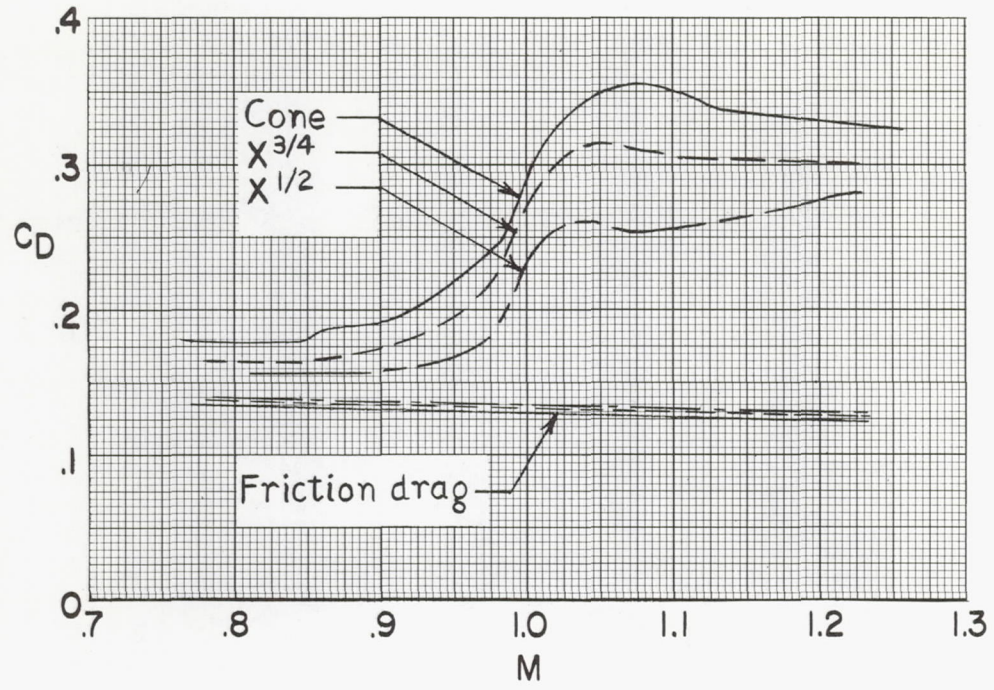

(a) Power series.

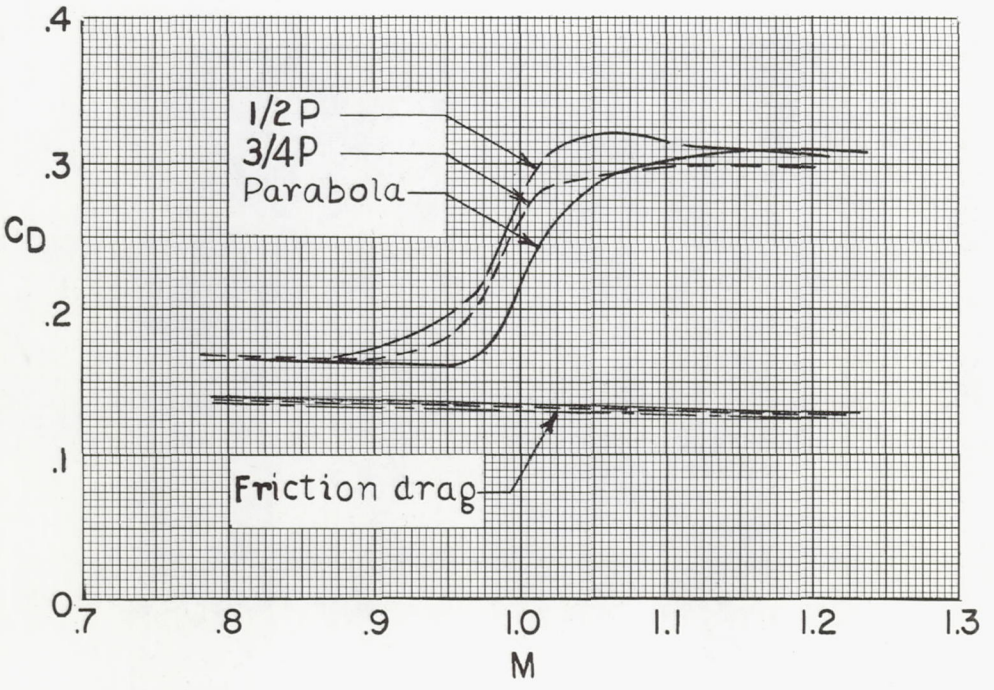

(b) Parabolic series.

Figure 3.- Total-configuration drag coefficients.

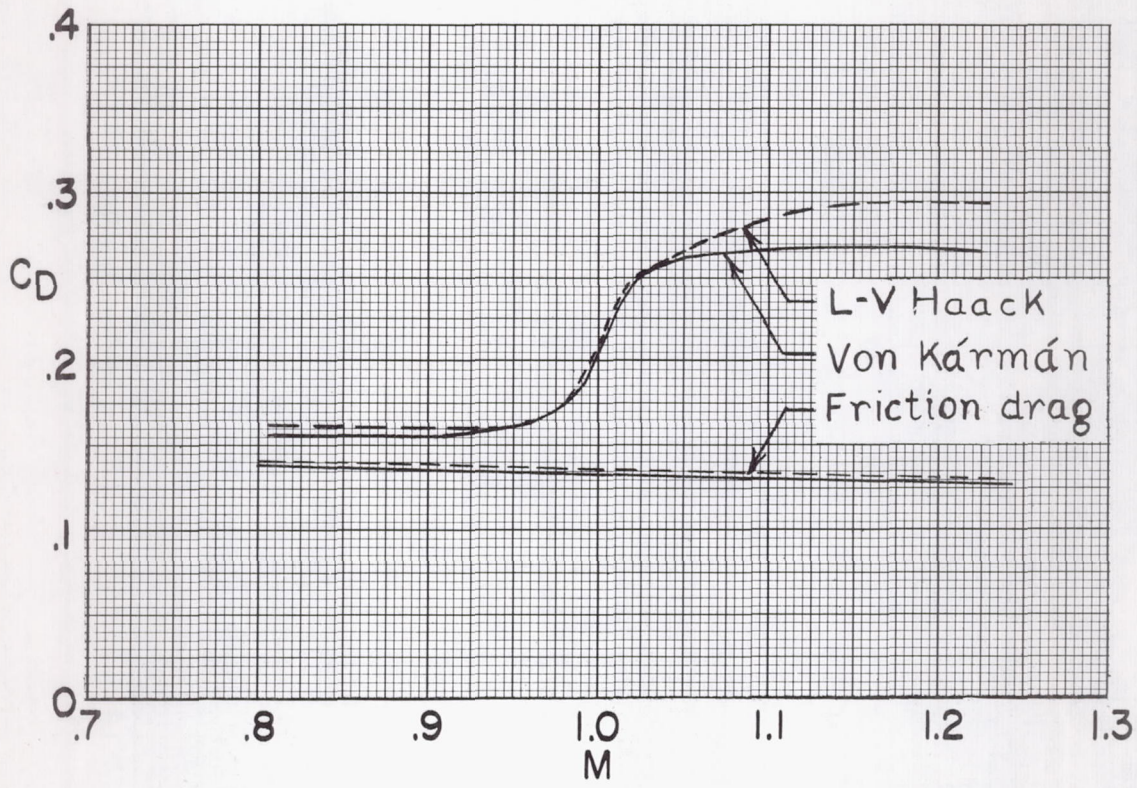

(c) Haack series.

Figure 3.- Concluded.

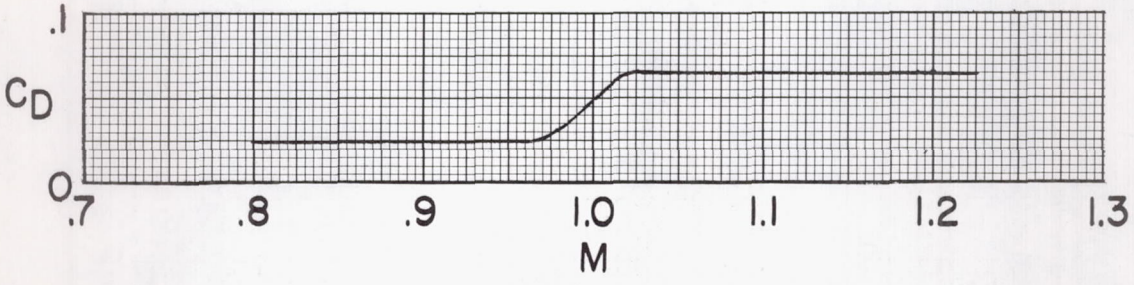

Figure 4.- Tare drag.

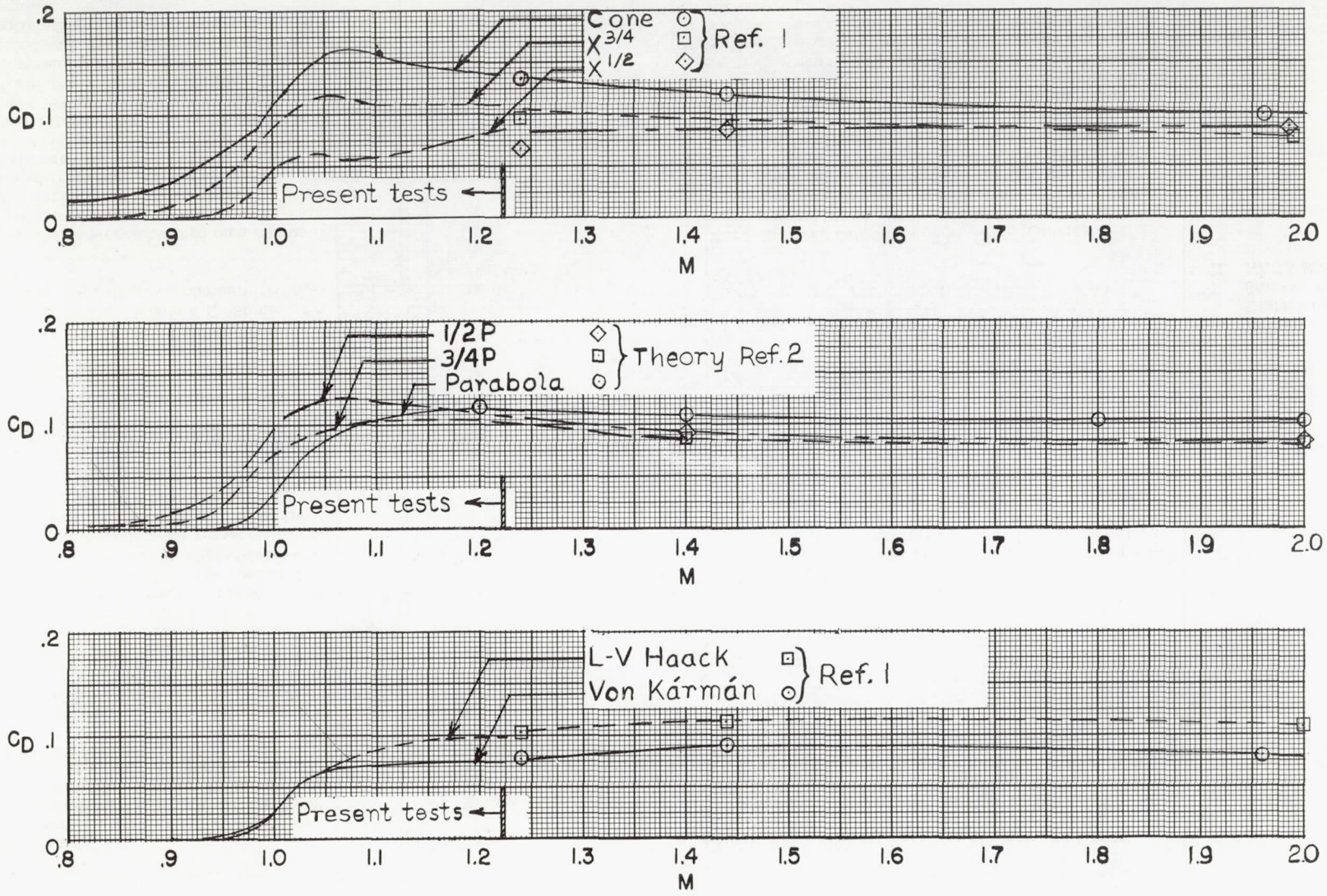

Figure 5.- Nose pressure drag coefficients.